(Invited) Point Defect Characterization of Group-III Nitrides by Using Monoenergetic Positron Beams

Article *in* ECS Transactions · May 2014

DOI: 10.1149/06105.0019ecst

CITATIONS
6

READS
470

5 authors, including:

Akira Uedono
University of Tsukuba
440 PUBLICATIONS **5,278** CITATIONS
SEE PROFILE

Oshima Nagayasu
National Institute of Advanced Industrial Science and Technology
123 PUBLICATIONS **1,139** CITATIONS
SEE PROFILE

Ryoichi Suzuki
National Institute of Advanced Industrial Science and Technology
466 PUBLICATIONS **5,993** CITATIONS
SEE PROFILE

Masatomo Sumiya
National Institute for Materials Science
147 PUBLICATIONS **4,468** CITATIONS
SEE PROFILE

ECS Transactions, 61 (5) 19-30 (2014)
10.1149/06105.0019ecst ©The Electrochemical Society

Point defect characterization of group-III nitrides by using monoenergetic positron beams

Akira Uedono[a], Shoji Ishibashi[b], Nagayasu Oshima[c], Ryoichi Suzuki[c], and Masatomo Sumiya[d]

[a] Division of Applied Physics, Faculty of Pure and Applied Science, University of Tsukuba, Tsukuba, Ibaraki 305-8573, Japan
[b] Nanosystem Research Institute (NRI) "RICS", National Institute of Advanced Industrial Science and Technology (AIST), Tsukuba, Ibaraki 305-8568, Japan
[c] Research Institute of Instrumentation Frontier, National Institute of Advanced Industrial Science and Technology, Tsukuba, Ibaraki, 305-8568, Japan
[d] Wide Bandgap Material Group, National Institute for Materials Science, 305-0044, Tsukuba, Japan

Positron annihilation is a powerful technique for evaluating point defects in semiconductors. Using this technique, one can detect vacancy-type defects in subsurface regions with high-sensitivity. We have used monoenergetic positron beams to probe native vacancies in $In_xGa_{1-x}N$ grown on sapphire and GaN substrates by metalorganic vapor phase epitaxy. It was found that vacancy-type defects were introduced with increasing InN composition, and the major defect species was identified as complexes between a cation vacancy and a nitrogen vacancy. The concentration of the defects was found to be suppressed by Mg doping, suggesting that Mg is an excellent suppressor of cation vacancies in $In_xGa_{1-x}N$. The crystal quality of the $In_xGa_{1-x}N$ films was greatly improved using the GaN substrate, but point defects, especially vacancy-type defects were found to present in the film.

Introduction

Grope-III nitride semiconductors are a key material to fabrications of light-emitting diodes (LEDs), laser diodes (LDs), and photodetectors.[1,2)] Because the recent progress of such optical devices mainly based on developments of growth technologies of GaN and Ga-rich $In_xGa_{1-x}N$, many studies have been carried out on those alloys. The potential of $In_xGa_{1-x}N$ as the optical material mainly comes from the ability to control band gaps from 0.65 eV to 3.43 eV, which correspond to entire wavelengths from infrared to ultraviolet regions. Because those band gap energies can cover the solar spectrum, $In_xGa_{1-x}N$ is also recognized as having a high potential as a photovoltaic device material.[3)] The external quantum efficiency (EQE) of an $In_xGa_{1-x}N$-based LED is known to drop rapidly with increasing InN composition x. The EQE decrease is attributed to (i) piezoelectric fields in multiplayer structures which cause a separation between electron and hole wavefunctions, and (ii) the degradation of crystal quality. For $In_xGa_{1-x}N$-based tandem solar cells, the degradation of conversion efficiency also occurs when x increases.[4-7)] In addition, fabricating the solar cells requires overcoming several challenges such as the formation of thick $In_xGa_{1-x}N$ layers, quality control of interfaces in multilayered structures, and *p*-type doping. During

growth of $In_xGa_{1-x}N$ layers, the large difference in the lattice constants of InN and GaN cause unusually high strain to be introduced into the layer, and this causes dislocations, stacking faults, misorientations, phase separations, etc.[8-11] Native point-defects are also known to act as non-radiative recombination centers in group-III nitrides. Thus, further knowledge regarding such defects is needed to improve the optical and electrical properties of $In_xGa_{1-x}N$-based optical devices and solar cells. Positron annihilation is a powerful technique for evaluating vacancy-type defects in semiconductors,[12] and the defects in group-III nitrides have been investigated using this method.[13-18] In the present study, we have used monoenergetic positron beams to probe native vacancies in $In_xGa_{1-x}N$ (x = 0.08 and 0.14) grown by metalorganic chemical vapor deposition (MOCVD).

Analysis method –basics of positron annihilation –

Positrons can be obtained from the β^+-decay of radioactive isotopes, e.g. from ^{22}Na (Fig. 1).[12] When a positron is implanted into condensed matter, it annihilates with an electron and emits two γ quanta. The energy of such annihilation γ-rays E_γ can be obtained by the relation: $E_\gamma = m_0c^2 = 511$ keV, where m_0 and c are positron mass and speed of light. The energy distribution of the γ rays is broadened by the momentum component of the annihilating electron-positron pair p_L, which is parallel to the emitting direction of the γ rays. The energy of the γ rays is given by $E_\gamma = m_0c^2 \pm \Delta E_\gamma$. Here, the Doppler shift ΔE_γ is given by $\Delta E_\gamma = p_Lc/2$. The typical Doppler broadening spectrum for GaN is shown in Fig. 2. The solid curves represent the spectra for the annihilation of positrons with core and valence electrons, where those curves were obtained by our in-house code, which uses valence-electron wavefunctions determined by the projector augmented-wave (PAW) method.[19] In Fig. 2, the broader spectrum for core electrons corresponds to the broadened momentum distribution of such electrons. As shown in Fig. 1, a freely diffusing positron may be localized in a vacancy-type defect because of Coulomb repulsion from positively charged ion cores. Because the momentum distribution of the electrons in such defects differs from that of electrons in the bulk material, these defects can be detected by measuring the Doppler broadening spectra of the annihilation radiation.

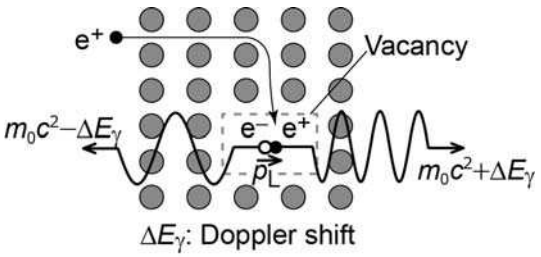

Figure 1. Scheme of positron annihilation experiments. Positrons from an isotope source (^{22}Na) penetrate the sample. After thermalization of energetic positrons, they diffuse in the sample before the annihilation. Positrons could be trapped by vacancy-type defects before annihilation. The energy distribution of the annihilation γ rays is broadened by the momentum component of the annihilating electron-positron pair p_L, which is parallel to the emitting direction of the γ rays.

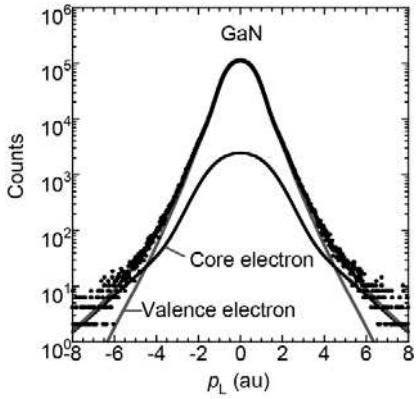

Figure 2. Doppler broadening spectrum for GaN. The solid curves correspond to the annihilation of positrons with core and valence electrons, respectively.

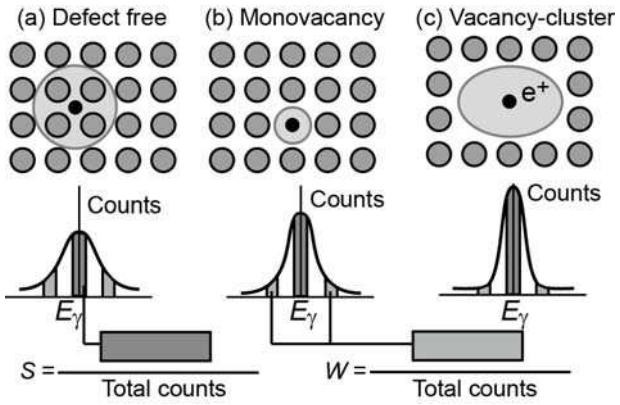

Figure 3. Schematic drawing of Doppler broadening spectrum for (a) the annihilation of positrons from delocalized state. The spectra for annihilation of positrons trapped by (b) a monovacancy and (c) a vacancy-cluster are also shown. The Doppler broadening spectrum is characterized by the *S* parameter, which mainly reflects changes due to the annihilation of positron-electron pairs with a low-momentum distribution, and by the *W* parameter, which mainly characterizes changes due to the annihilation of pairs with a high-momentum distribution.

The resultant changes in the spectra are characterized by the *S* parameter, which mainly reflects changes due to the annihilation of positron-electron pairs with a low-momentum distribution, and by the *W* parameter, which mainly characterizes changes due to the annihilation of pairs with a high-momentum distribution. The definitions of *S* and *W*, and the change in the Doppler broadened spectra due to the trapping of positrons are shown in Fig. 3 schematically. In general, the characteristic value of *S* (*W*) expected for the annihilation of positrons due to their trapping by vacancy-type defects is larger (smaller) than that for positrons annihilated from the free-state. For group-III nitrides, because an isolated nitrogen vacancy (V_N) is positively charged, the major trapping center of positrons is cation monovacancies (V_M) such as the In vacancy (V_{In}) and Ga vacancy (V_{Ga}) or their complexes such as $V_{In}V_N$ and $V_{Ga}V_N$. Positron densities around (a) defect-free GaN, (b) V_{Ga}, and (c) V_N are shown in Fig. 4, where gray and black circles correspond to Ga- and N-atoms. It can be seen that positrons strongly are localized by the trapping of positrons by V_{Ga}, but they are repelled from V_N.

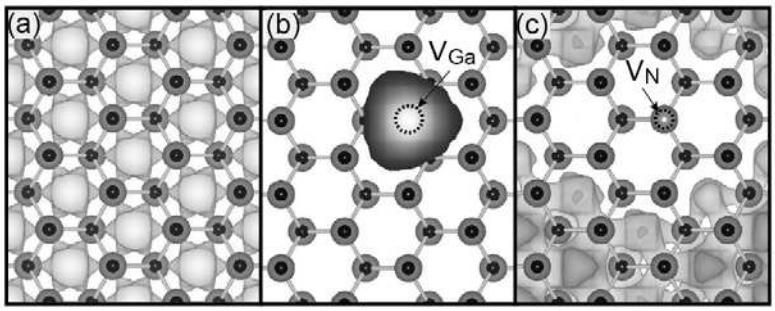

Figure 4. Positron densities around (a) defect-free GaN, (b) V_{Ga}, and (c) V_N. Gray and black circles correspond to Ga- and N-atoms. The distributions of positrons were calculated using our in-house code, which uses valence-electron wavefunctions determined by the PAW method.[19)]

Experiment

The samples investigated were $In_xGa_{1-x}N$ (x = 0.08 and 0.14) grown on sapphire substrates using MOCVD. The growth method and the optical properties of the samples are described elsewhere.[20)] Ammonia, trimethylgallium, trimethylindium, and bis(methylcyclopentadienyl)-magnesium ($MeCp_2Mg$) were used as nitrogen, Ga, In, and Mg sources, respectively. 1.4-μm-thick GaN films were grown on *c*-plane sapphire substrates at 1000°C with buffer layers, and then 300-nm-thick $In_{0.08}Ga_{0.92}N$ film was grown. For $In_{0.14}Ga_{0.86}N$(300 nm), the film was deposited on Mg-doped GaN(120 nm)/GaN/sapphire substrate. The growth temperatures of the $In_{0.08}Ga_{0.92}N$, $In_{0.14}Ga_{0.86}N$, and Mg-doped $In_{0.08}Ga_{0.92}N$ (Mg: $In_{0.08}Ga_{0.92}N$) were 800, 790, and 800°C, respectively. In order to know an effect of the substrate on the crystalline quality of $In_xGa_{1-x}N$, we used bulk-GaN as the substrate in the present experiments. Before the deposition of the film, 1.5-μm-thick GaN film was grown on the substrate. Then, 225-nm-thick $In_{0.08}Ga_{0.92}N$ deposited on the template ($In_{0.08}Ga_{0.92}N$/GaN), where the substrate temperature was kept at 830°C for an initial growth of the film (75-nm), then it was decreased to 780°C.

Hall measurements were conducted using the ResiTest 8300 system (TOYO). The electron and hole concentrations of undoped and Mg-doped InGaN were $n_e = 5\times10^{17}$ cm^{-3} and $n_p = 5\times10^{18}$ cm^{-3}, respectively. The structural properties of the samples were investigated by high-resolution x-ray diffraction (XRD) reciprocal space mapping (RSM) using PaNalytical X'Pert Pro. Photoluminescence (PL) spectra were measured using a 325-nm He-Cd laser as an excitation source and a Perkin-Elmer Lambda 950 UV-Vis-NIR spectrophotometer. From observed PL spectra, the InN fraction x in the film was determined. Table I shows the FWHM of (0002)- and $(10\bar{1}1)$-peaks obtained by ω-scanning measurements (the detector remained stationary and the sample was rotated about the ω axis). For $In_{0.14}Ga_{0.86}N$, the results for $(10\bar{1}1)$-peak is not shown because broadened multiple peaks were observed. From the table, the FWHM values for the $In_{0.08}Ga_{0.92}N$ film grown on the GaN substrate were smaller than those for the films grown on the sapphire temperate, suggesting that the quality of the substrate is one of crucial parameters to obtain high-quality $In_xGa_{1-x}N$ film.

.

TABLE I. FWHM of (0002) and (10 $\bar{1}$ 1)-peaks obtained by ω-scanning measurements. The obtained small FWHM values for $In_{0.08}Ga_{0.92}N$/GaN suggests an improvement of the crystal quality of $In_{0.08}Ga_{0.92}N$ film by using the GaN substrate.

Sample	(0002) (°)	(10 $\bar{1}$ 1) (°)
$In_{0.08}Ga_{0.92}N$	0.088	0.21
$In_{0.14}Ga_{0.86}N$	0.13	-
Mg:$In_{0.08}Ga_{0.92}N$	0.077	0.17
$In_{0.08}Ga_{0.92}N$/GaN	0.014	0.043

With a monoenergetic positron beam, Doppler broadening spectra of the annihilation radiation were measured with a Ge detector as a function of the incident positron energy E. A detail of this technique is described elsewhere.[21,22] The low-momentum part of the spectra was characterized by the S parameter, defined as the number of annihilation events over the energy range of 511 keV ± $\Delta E_{\gamma\text{-width}}$ (where $\Delta E_{\gamma\text{-width}}$ = 0.76 keV) around the center of the peak, and the high-momentum part was characterized using the W parameter, defined as the annihilation events in the range of 3.4 keV ≤ $|\Delta E_{\gamma\text{-width}}|$ ≤ 6.8 keV. Doppler broadening profiles with 5×10^6 counts were also measured using a coincidence system. The relationship between S and E was analyzed by VEPFIT, a computer program developed by van Veen *et al*.[23] The S–E curve was fitted using

$$S(E) = S_e F_e(E) + S_s F_s(E) + \Sigma S_i F_i(E), \quad (1)$$

where $F_e(E)$ is the fraction of non-thermalized (epithermal) positrons annihilated at the surface, and $F_s(E)$ and $F_i(E)$ are the fractions of thermalized positrons annihilated at the surface and in the i-th layer, respectively; ($F_e(E) + F_s(E) + \Sigma F_i(E)$=1). S_e, S_s, and S_i are S parameters that correspond respectively to the annihilation of epithermal positrons at the surface, that of thermalized positrons at the surface, and that of thermalized positrons in the i-th block.

Doppler broadening spectra corresponding to the annihilation of positrons annihilated from the delocalized state and that of positrons trapped by typical vacancies in $In_{0.125}Ga_{0.875}N$ were theoretically calculated using our in-house QMAS (Quantum MAterials Simulator) code,[19] which uses valence-electron wavefunctions determined by the projector augmented-wave (PAW) method.[24-26] To calculate the exchange and correlation energy of electrons, generalized gradient approximation was used.[28] The plane-wave cut-off energy was set to 20 hartree. The electron-positron correlation energy is expressed with the local-density-approximation formalism[28] or its modified version for semiconductors.[29] Doppler broadening spectra were calculated using the enhancement factor corresponding to the correlation-energy expression. The initial bulk structure containing 128 atoms has been generated by means of the special-quasirandom-structure (SQS) approach.[30,31] Atomic positions were then optimized by first-principles quenched molecular dynamics. For structures containing a vacancy, one atom was removed from the optimized bulk structure and the positions of the remaining atoms were optimized. Eighteen cation vacancies were selected in the present calculation. After simulating Doppler broadening spectra, they were characterized by S and W. The simulation was also performed for "ordered" $In_{0.5}Ga_{0.5}N$, where In- and Ga-faces were assumed to alternately locate in c-faces. The values of S and W for $In_{0.125}Ga_{0.875}N$ were then obtained by interpolation between the values for GaN and $In_{0.5}Ga_{0.5}N$.

Results and discussion

Figure 1 shows XRD RSMs for the (a) $In_{0.08}Ga_{0.92}N$, (b) $In_{0.14}Ga_{0.86}N$, (c) Mg: $In_{0.08}Ga_{0.92}N$, and (c) $In_{0.08}Ga_{0.91}N$/GaN measured around the $(10\bar{1}4)$-plane. For the $In_{0.08}Ga_{0.92}N$ films grown on the sapphire and GaN substrates, the maximum of the diffraction peak was nearly aligned with the GaN diffraction maximum along Q_x, the reciprocal space vector in the plane of the layers. For the $In_{0.14}Ga_{0.86}N$ film, the observed downward and left-hand-side shift of the peak suggests lattice relaxation. This also correlates to the broadened peaks observed in the ω-scanning measurements (Table I). For $In_{0.08}Ga_{0.91}N$/GaN, observed two peaks corresponding to the film can be associated with the variation of the InN fraction in the film which was introduced by the different growth temperatures (780 and 830°C).

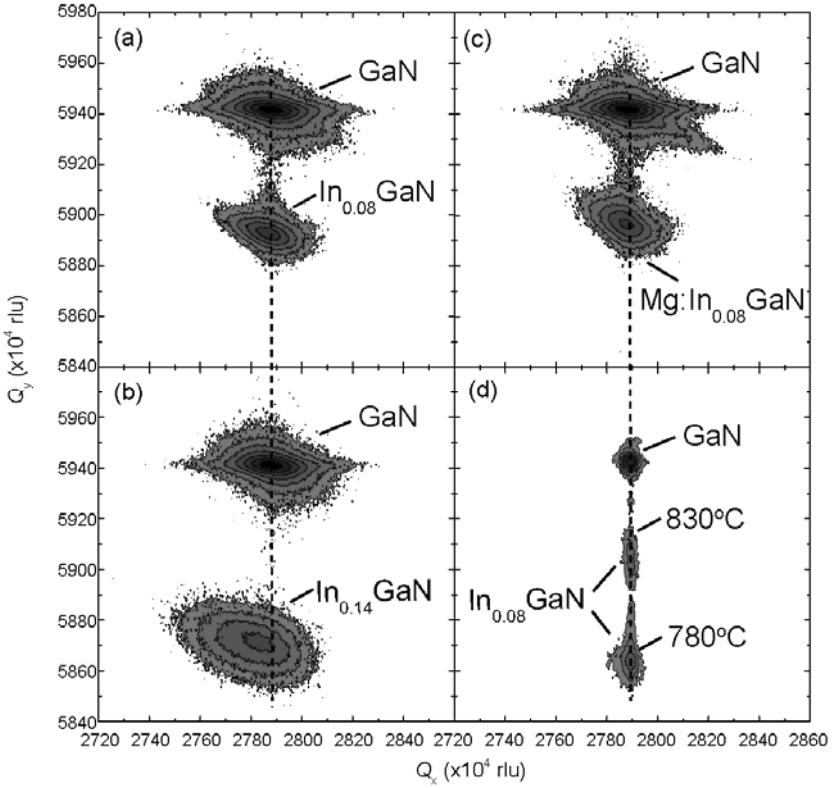

Figure 5. XRD $(10\bar{1}4)$-plane RSMs for (a) the $In_{0.08}Ga_{0.92}N$, (b) $In_{0.14}Ga_{0.86}N$, (c) Mg:$In_{0.08}Ga_{0.92}N$, and (d) $In_{0.08}Ga_{0.92}N$/Si (rlu: reciprocal lattice unit). The peaks corresponding to the $In_xGa_{1-x}N$ and GaN layers are shown in the figure.

Figure 6 shows the S values of $In_xGa_{1-x}N$ grown on the sapphire and GaN substrates as a function of incident positron energy E. The S–E curves for GaN grown by hydride vapor phase epitaxy (HVPE) are also shown. The mean implantation depth of positrons is shown in the upper horizontal axis. For HVPE-GaN, the S value increased with decreasing E, which corresponds to the diffusion of positrons toward the surface, where the large S values at low E ($\cong$ 0.1 keV) are associated with the annihilation of positrons at the surface. The S value saturated at E > 20 keV, suggesting that almost all positrons annihilate in the bulk in this energy range. This S value was close to that previously reported for defect-free HVPE-GaN.[14] The observed S–E curve was fitted using eq. (1), and the solid curve is a fit

to the experimental data. The diffusion length of positrons was obtained as 72± 1 nm, and this is a typical value for defect-free GaN.[14)]

For Mg:$In_{0.08}Ga_{0.92}N$, the *S* value near the surface (< 1 keV) decreased rapidly with increasing *E*. This is the typical behavior of *S* for *p*-type GaN,[32)] and was attributed to the suppression of positron diffusion toward the surface due to band bending near the surface. For $In_{0.14}Ga_{0.86}N$, the *S* value was almost flat at *E* = 1-3 keV, which suggests that almost all positrons annihilated in the layer without diffusing back to the surface. For all samples grown on the sapphire substrate, dips in the *S*–*E* curves were observed at *E* = 10-15 keV, which can be attributed to the annihilation of positrons near the $In_xGa_{1-x}N$/GaN interface.

Annihilation characteristics of positrons in layered structures can be discussed through graphical analysis of the relationship between the *S* and *W* parameters.[12)] Figure 7 shows the *S*–*W* relationship for the samples shown in Fig. 6. The (*S*,*W*) value for HVPE-GaN (defect-free GaN) is also shown. Arrows show directions of the increase of *E*. For Mg:$In_{0.08}Ga_{0.92}N$ [Fig. 7(c)], the (*S*,*W*) trajectory can be represented by a straight line (reference line). The value approached the defect-free (*S*,*W*) value for GaN with increasing *E* (*E* ≤ 10 keV). The difference between them became small at *E* = 10 keV (this energy corresponds to the dip in the *S*–*E* curve). For $In_{0.14}Ga_{0.86}N$ [Fig. 7(b)], although the (*S*,*W*) value saturated at *E* = 2.9-5.4 keV (corresponding to the $In_{0.14}Ga_{0.86}N$ layer), above *E* = 5.9 keV it started to approach the defect-free (*S*,*W*) value. The saturation of the (*S*,*W*) value can be attributed to the trapping of positrons by vacancy-type defects in the film. From the observed behavior of (*S*,*W*), the momentum distribution of electrons near the $In_xGa_{1-x}N$/GaN interface is considered to be close to that for defect-free $In_xGa_{1-x}N$ or GaN.

The *S*–*E* curves were fitted using Eq. (1). In the fitting, the region sampled by the positrons was divided into blocks corresponding to the positron annihilation in the $In_xGa_{1-x}N$ layer, the $In_xGa_{1-x}N$/GaN interface, the GaN layer, and the substrate. The widths of the blocks and the corresponding *S* values were determined by the fitting. From the results shown in Fig. 7, however, the *S* value for the second block was fixed as the *S* value for HVPE-GaN. The solid curves in Fig. 6 are fits to the experimental data, and the derived depth distributions of *S* are shown in Fig. 8.

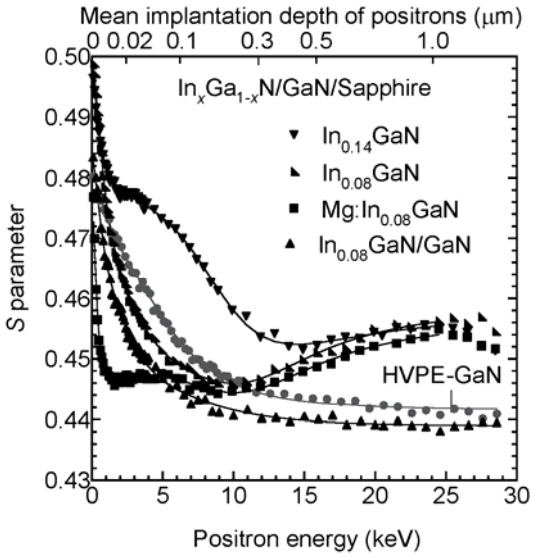

Figure 6. *S* parameters as a function of incident positron energy *E* for the $In_xGa_{1-x}N$ layers grown on the sapphire and GaN substrates. The solid curves are fittings of the diffusion equation for positrons to the experimental data.

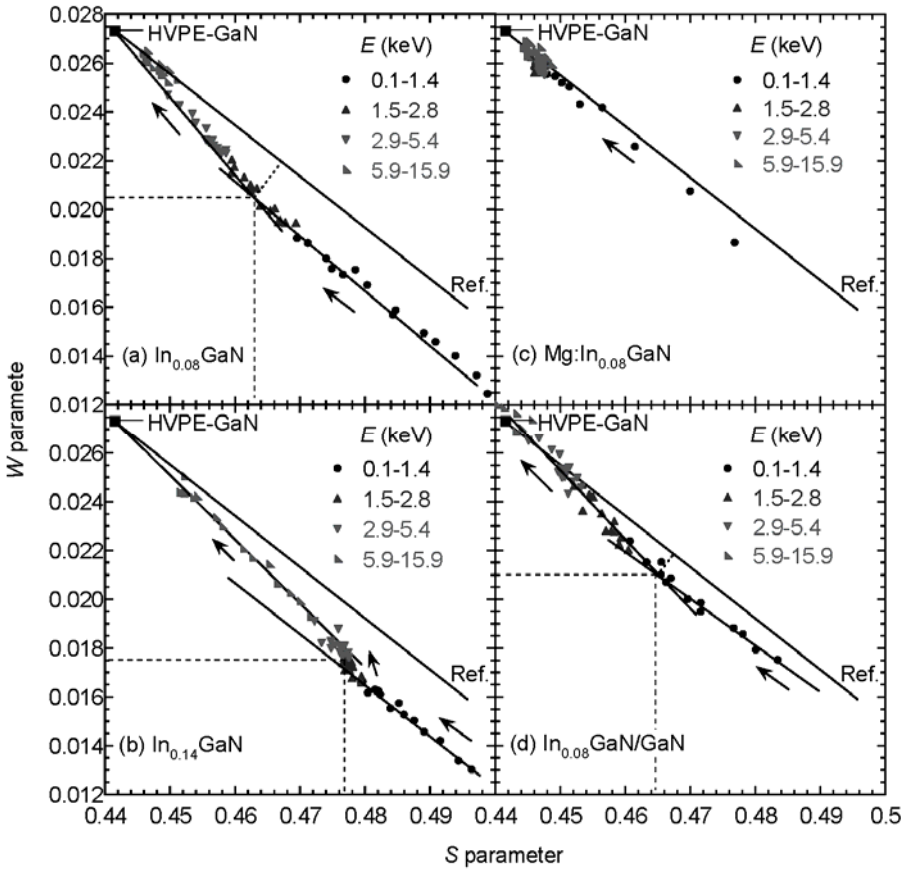

Figure 7. Relationships between S and W measured at $E \leq 15.9$ keV for (a) $In_{0.08}Ga_{0.92}N$, (b) $In_{0.14}Ga_{0.86}N$, (c) Mg:$In_{0.08}Ga_{0.92}N$, and (d) $In_{0.08}Ga_{0.92}N$/Si. Arrows show directions of the increase of E. The (S,W) value for HVPE-GaN is also shown. For Mg:$In_{0.08}Ga_{0.92}N$, the (S,W) values located on a line, and this is used as a reference for other samples.

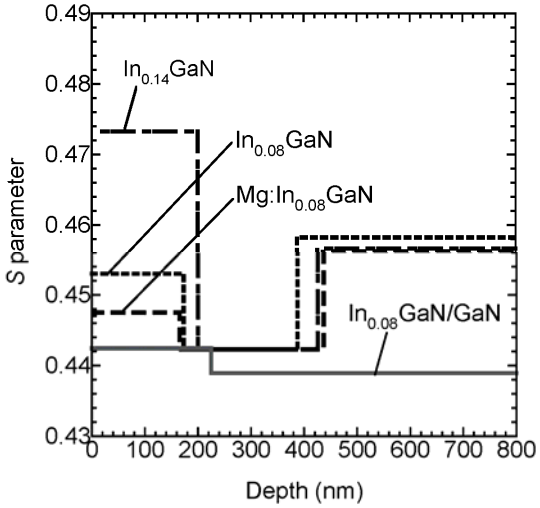

Figure 8. Depth distributions of S for $In_xGa_{1-x}N$ (x=0.08 and 0.14) grown on the sapphire and GaN substrates derived from the fitting (Fig. 6).

For all samples grown on the sapphire substrate, although the second block represents the $In_xGa_{1-x}N$/GaN interface, their widths were obtained as about 200 nm. Makkonen *et al.*[18] reported the localization of positrons at the InGaN/GaN interface due to the built-in electric field caused by the piezoelectric effect. Because this effect was not included in the fitting model, the accumulation of positrons near the interface appeared as the wide width of the second block. In Fig. 8, the *S* value in Mg:$In_{0.08}Ga_{0.92}N$ was small (first block). This shows that Mg doping suppresses cation vacancy introduction. For undoped $In_xGa_{1-x}N$, the *S* value increased with increasing *x*, suggesting the introduction of cation vacancies into the layers.

For $In_{0.08}Ga_{0.92}N$/GaN, the *S* value for the film is lower than the undoped $In_{0.08}Ga_{0.92}N$ film grown on the sapphire substrate, suggesting an improvement of the film quality by using the GaN substrate. In Fig. 7(a), for the $In_{0.08}Ga_{0.92}N$ film grown on the sapphire substrate, the (*S*,*W*) values at $E \cong 3$ keV were found to locate in the left-hand side region from the reference line, where the difference was shown as a dotted line. This is due to the annihilation of positrons trapped by vacancy-type defects in the film. For $In_{0.08}Ga_{0.92}N$/GaN [Fig. 7(d)], a similar behavior of the (*S*,*W*) value was observed. As shown in Fig. 1, the crystalline quality of the $In_xGa_{1-x}N$ seems to be greatly improved by using GaN substrates, but we can conclude that vacancy-type defects still exist in the film.

Figure 9 shows the (*S*,*W*) values calculated from the coincidence Doppler broadening spectra using the PAW method. The values correspond to the annihilation of positrons in the delocalized state (defect-free: DF) in ordered $In_{0.125}Ga_{0.875}N$ and those of positrons trapped by Ga-vacancy V_{Ga} and divacancy ($V_{Ga}V_N$) (blue symbol) are shown. The result for DF-GaN is also shown. Arrows show the effect of N-vacancy V_N coupled with V_{Ga}. The (*S*,*W*) values calculated using SQS for DF-$In_{0.125}Ga_{0.875}N$ and cation vacancies are also shown. The (*S*,*W*) values calculated using the ordered structure and SQS are close to each other, suggesting that the (*S*,*W*) values calculated using ordered-$In_{0.125}Ga_{0.875}N$ can be used to compare with experimentally obtained values. Using the coincidence system, the (*S*,*W*) values were measured at $E = 3$ keV for $In_{0.14}Ga_{0.86}N$, at $E = 3$ and 9 keV for Mg:$In_{0.08}Ga_{0.92}N$, and at $E = 30$ keV for HVPE-GaN. For $In_{0.14}Ga_{0.86}N$, the obtained value is located on the right side of the line connecting the values of the defect-free and $V_{Ga}V_N$. Because the formation of vacancy complexes with V_N causes a rightward shift in the *S*–*W* plot, the major trapping center of positrons can be determined as complexes between a cation vacancy and V_Ns. For Mg:$In_{0.08}Ga_{0.92}N$, the measured (*S*,*W*) values are located on the line connecting the values of $In_{0.14}Ga_{0.86}N$ and HVPE-GaN. Thus, the major defect species is expected to be the same as that for $In_{0.14}Ga_{0.86}N$, but their concentration was suppressed by Mg-doping.

Using first-principles calculation,[33] it was reported that the formation energy of V_N decreased as the number of In adjacent to V_N increased. Thus, both the bond-length/angle distortions and the decrease in the formation energy of V_N are expected to promote the introduction of V_N with increasing InN content. Although positrons are not trapped by isolated V_N, some of them preferentially couple with cation vacancies and form stable complexes. Thus, we can conclude that the observed behaviour of defects in in $In_xGa_{1-x}N$ is considered to be the introduction of V_N and related formation of cation-vacancy-V_N complexes.

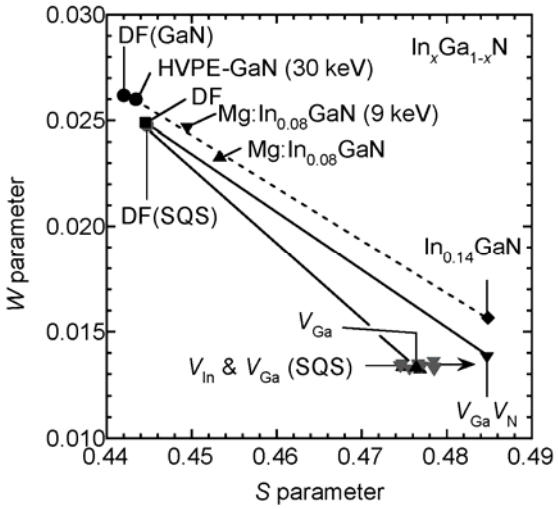

Figure 9. (*S*,*W*) values corresponding to the annihilation of positrons in the delocalized state (defect-free: DF) and that of positrons trapped by V_{Ga} as calculated for $In_{0.125}Ga_{0.875}N$. The result for DF-GaN is also shown. Arrows show the effect of V_N coupled with V_{Ga}. The (*S*,*W*) values for $In_{0.14}Ga_{0.86}N$, Mg-doped $In_{0.08}Ga_{0.92}N$, and HVPE-GaN are also shown.

Conclusion

We studied vacancy-type defects in $In_xGa_{1-x}N$ grown on the sapphire and GaN substrates by MOCVD. Doppler broadening spectra were measured as a function of the incident energy of positrons for $In_xGa_{1-x}N$ grown on GaN. Coincidence Doppler broadening spectra were also measured and compared with spectra simulated using the PAW method. The major defect species in the $In_xGa_{1-x}N$ film was identified as cation vacancies coupled with V_N and their concentration increased with increasing In content. The cation vacancy concentration, however, was found to be decreased by Mg doping. The film quality was greatly improved by using the GaN substrate, but vacancy-type defects are still observed using positron annihilation. We have shown that the positron annihilation parameter is sensitive to vacancy-type defects in $In_xGa_{1-x}N$ films in InGaN/GaN layered structures, meaning that this technique can be a useful tool for evaluating InGaN-based devices.

Acknowledgements

Part of this study was financially supported by the Advanced Low Carbon Technology Research and Development Program, Japan Science and Technology Agency.

References

1. J. Wu, J. Appl. Phys. **106**, 011101 (2009).
2. R. Haitz and J. Y. Tsao, phys. stat. sol. A **208**, 17 (2011).
3. J. Wu, W. Walukiewicz, K. M. Yu, W. Shan, J. W. Ager III, E. E. Haller, H. Lu, W. J. Schaff, W. K. Metzger, and S. Kurtz, J. Appl. Phys. **94**, 3967 (2003).
4. O. Jani, I. Ferguson, C. Honsberg, and S. Kurtz, Appl. Phys. Lett. **91**, 132117 (2007).
5. X. Chen, K. D. Matthews, D. Hao, W. J. Schaff, and L. F. Eastman, phys. stat. sol. (a) **205**, 1103 (2008).

6. L. Sang, M. Liao, N. Ikeda, Y. Koide, and M. Sumiya, Appl. Phys. Lett. **99**, 161109 (2011).
7. M. Mori, S. Kondo, S. Yamamoto, T. Nakao, T. Fujii, M. Iwaya, T. Takeuchi, S. Kamiyama, I. Akasaki, and H. Amano, Appl. Phys. Exp. **6**, 082301 (2013).
8. R. Liu, J. Mei, S. Srinivasan, F. A. Ponce, H. Omiya, Y. Narukawa, and T. Mukai, Appl. Phys. Lett. **89**, 201911 (2006).
9. S. W. Lee, D. C. Oh, H. Goto, J. S. Ha, H. J. Lee, T. Hanada, M. W. Cho, T. Yao, S. K. Hong, H. Y. Lee, S. R. Cho, J. W. Choi, J. H. Choi, J. H. Jang, J. E. Shin, and J. S. Lee, Appl. Phys. Lett. **89**, 132117 (2006).
10. Q. Dai, M. F. Schubert, M. H. Kim, J. K. Kim, E. F. Schubert, D. D. Koleske, M. H. Crawford, S. R. Lee, A. J. Fischer, G. Thaler, and M. A. Banas, Appl. Phys. Lett. **94**, 111109 (2009).
11. Y. Kuwahara, T. Fujii, Y. Fujiyama, T. Sugiyama, M. Iwaya, T. Takeuchi, S. Kamiyama, I. Akasaki, and H. Amano, Appl. Phys. Exp. **3**, 111001 (2010).
12. R. Krause-Rehberg and H. S. Leipner, Positron Annihilation in Semiconductors, Solid-State Sciences (Springer-Verlag, Berlin, 1999) vol. 127.
13. K. Saarinen, T. Laine, S. Kuisma, J. Nissilä, P. Hautojärvi, L. Dobrzynski, J. M. Baranowski, K. Pakula, R. Stepniewski, M. Wojdak, A. Wysmolek, T. Suski, M. Leszczynski, I. Grzegory, and S. Porowski, Phys. Rev. Lett. **79**, 3030 (1997).
14. A. Uedono, S. F. Chichibu, Z. Q. Chen, M. Sumiya, R. Suzuki, T. Ohdaira, T. Mikado, T. Mukai, and S. Nakamura, J. Appl. Phys. **90**, 181 (2001).
15. S. Hautakangas, K. Saarinen, L. Liszkay, J. A. Freitas, Jr., and R. L. Henry, Phys. Rev. B **72**, 165303 (2005).
16. F. Tuomisto, A. Pelli, K. M. Yu, W. Walukiewicz, and W. J. Schaff, Phys. Rev. B **75**, 193201 (2007).
17. T. Onuma, A. Uedono, H. Asamizu, H. Sato, J. F. Kaeding, M. Iza, S. P. DenBaars, S. Nakamura, and S. F. Chichibu, Appl. Phys. Lett. **96**, 091913 (2010).
18. I. Makkonen, A. Snicker, M. J. Puska, J.-M. Mäki, and F. Tuomisto, Phys. Rev. B 82, 041307(R) (2010).
19. S. Ishibashi, Materials Science Forum **445-446**, 401 (2004). Detailed and up-to-date information of QMAS is reported in http://qmas.jp/.
20. L. Sang, M. Liao, N. Ikeda, Y. Koide, and M. Sumiya, Appl. Phys. Lett. **99**, 161109 (2011).
21. A. Uedono, S. Ishibashi, T. Ohdaira, and R. Suzuki, J. Crystal Growth **311**, 3075 (2009).
22. A. Uedono, S. Ishibashi, N. Oshima, and R. Suzuki, Jpn. J. Appl. Phys. **52**, 08JJ02 (2013).
23. A. van Veen, H. Schut, J. de Vries, R. A. Hakvoort, and M. R. Ijpma, AIP Conf. Proc. **218**, 171 (1990).
24. P. E. Blöchl, Phys. Rev. B **50**, 17953 (1994).
25. N. A. W. Holzwarth, G. E. Matthews, R B. Dunning, A. R. Tackett, and Y. Zeng, Phys. Rev. B **55**, 2005 (1997).
26. G. Kresse and D. Joubert, Phys. Rev. B **59**, 1758 (1999).
27. J. P. Perdew, K. Burke, and M. Ernzerhof, Phys. Rev. Lett. **77,** 3865 (1996).
28. E. Boroński and R. M. Nieminen, Phys. Rev. B **34**, 3820 (1986).
29. M.J. Puska, S. Mäkinen, M. Manninen, and R.M. Nieminen, Phys. Rev. B **39**, 7666 (1989).
30. A. Zunger, S.-H. Wei, L. G. Ferreira, and J. E. Bernard, Phys. Rev. Lett. **65**, 353 (1990).

31. K. C. Hass, L. C. Davis, and A. Zunger, Phys. Rev. B **42**, 3757 (1990).
32. A. Uedono, S. Ishibashi, K. Tenjinbayashi, T. Tsutsui, K. Nakahara, D. Takamizu, and S. F. Chichibu, J. Appl. Phys. **111**, 014508 (2012).
33. T. Obata, J. Iwata, K. Shiraishi, and A. Oshiyama, J. Crystal Growth **311**, 2772 (2009).